DOI: 10.1002/anie.201205167

Methane Reforming

The Active Phase of Nickel/Ordered $Ce_2Zr_2O_x$ Catalysts with a Discontinuity ($x = 7$–8) in Methane Steam Reforming**

Mizuki Tada, Shenghong Zhang, Sachin Malwadkar, Nozomu Ishiguro, Jun-ichi Soga, Yasutaka Nagai, Keitaro Tezuka, Hideo Imoto, Shinya Otsuka-Yao-Matsuo, Shin-ichi Ohkoshi, and Yasuhiro Iwasawa**

In recent years, there has been a surge in interest in syngas (H_2/CO) and H_2 production technologies, which utilize a wide variety of hydrocarbon feed stocks, such as gasoline, diesel, LPG, natural gas, methanol, and bio-ethanol. Among fossil fuels, natural gas (≥ 90 vol% CH_4) is the ideal fuel, owing to its ready availability, high energy density, and wide distribution network; CH_4 activation and reforming provide attractive ways to produce syngas, which can be transformed to useful larger hydrocarbons. Catalysts based on both noble metals and other metals have been extensively studied for CH_4 steam reforming.[1,2] Noble-metal (Rh, Ru, Ir, Pd, and Pt) catalysts are active and stable; however, because of the limited supply and high cost of noble metals, much attention has been paid to the development of non-noble metal catalysts, among which nickel-based catalysts have attracted particular attention because of their similar mechanistic features to noble-metal catalysts.[3]

The strong C–H bonds of CH_4 (439 kJ mol^{-1})[4] and endothermic heat of reforming reactions necessitate high temperatures for practical CH_4 conversion, and thus stable catalysts that resist sintering under extreme operating conditions. In CH_4 steam reforming, coke formation that deactivates the catalyst is thermodynamically favored at a H_2O/CH_4 ratio less than 1.4. Thus, industrial CH_4 steam reforming is usually carried out at a H_2O/CH_4 ratio of 1.4 or greater.[5] Although catalytic CH_4 steam reforming at low H_2O/CH_4 ratios have many advantages from operational and energy-consuming viewpoints, conventional nickel-based catalysts suffer from severe carbon deposition under such conditions. Supports and additives (for example, CeO_2, ZrO_2, CeO_2-ZrO_2, and La_2O_3) have been used to confer catalysts with kinetic resistance to carbon deposition and Ni sintering because they enhance redox activity and thermal stability, thereby promoting steam reforming.[6] The efficient CH_4 upgrading has long been a challenge in fundamental research.[7]

Herein, we report the unique properties and active phase of a new Ni/ordered $Ce_2Zr_2O_x$ ($x = 7$–8) catalyst with a regular arrangement of Ce and Zr ions in CH_4 steam reforming to produce H_2 and CO at $H_2O/CH_4 = 1$. The catalytic performance of Ni/$Ce_2Zr_2O_x$ ($x = 7$–8) strongly depends on the phase and oxygen content of $Ce_2Zr_2O_x$, and it shows a unique discontinuity in catalytic activity at $x = 7.5$.

The 2 wt% Ni/pyrochlore-$Ce_2Zr_2O_7$ catalyst showed a remarkable performance in CH_4 steam reforming at 923 K at $H_2O/CH_4 = 1$ (Table 1). Ni/CeO_2, Ni/ZrO_2, and Ni/CeO_2-ZrO_2 reduced by H_2 were much less active and selective than Ni/$Ce_2Zr_2O_7$, and significant deactivation was observed probably owing to Ni sintering and carbon deposition. On the other hand, the Ni/pyrochlore-$Ce_2Zr_2O_7$ catalyst was stable, resulting in a remarkably high catalytic performance (for a typical 50 h performance, see the Supporting Information, Figure S4). At 973 K, the Ni/$Ce_2Zr_2O_7$ catalyst exhibited high CO selectivity of 96–98% and high H_2 selectivity of 96–99% at CH_4 and H_2O conversions of 92–94% and >96%, respectively.

Platinum, a typical noble metal active for CH_4 steam reforming, was supported on CeO_2, ZrO_2, or $Ce_2Zr_2O_7$, but the performance was not significantly enhanced by these types of supports, and the CH_4 conversion on these Pt-based catalysts ranged between 29% and 39%. For Pt-based catalysts, CH_4 steam reforming may be controlled by Pt rather than by the nature of the support.[1,8]

In the presence of 0.8% O_2 in the reaction feed, the Ni/$Ce_2Zr_2O_7$ catalyst also exhibited high H_2 selectivity (97–99%) at a CH_4 conversion of 93–94% for at least 10 h. No significant deactivation was observed. These are great advan-

[*] Dr. M. Tada, Dr. S. Zhang, N. Ishiguro
Institute for Molecular Science
38 Nishigo-naka, Myodaiji, Okazaki, Aichi 444-8585 (Japan)
E-mail: mtada@ims.ac.jp
Dr. M. Tada
The Graduate University of Advanced Studies (SOKENDAI)
38 Nishigo-naka, Myodaiji, Okazaki, Aichi 444-8585 (Japan)
Dr. S. Malwadkar, Prof. Dr. Y. Iwasawa
The University of Electro-Communications
Chofu, Tokyo 182-8585 (Japan)
E-mail: iwasawa@pc.uec.ac.jp
N. Ishiguro, J. Soga, Prof. Dr. S. Ohkoshi
Department of Chemistry, Graduate School of Science, The University of Tokyo (Japan)
Dr. Y. Nagai
Toyota Central R&D Labs. Inc. (Japan)
Dr. K. Tezuka, Prof. Dr. H. Imoto
Department of Applied Chemistry, Utsunomiya University (Japan)
Prof. Dr. S. Otsuka-Yao-Matsuo
Graduate School of Engineering, Osaka University (Japan)

[**] This work was supported by the Funding Program for Next Generation World-Leading Researchers (GR090) from the Cabinet Office, Government of Japan, a Grant-in-Aid for Scientific Research (S) (No. 18106013) from MEXT (Japan), and the Joint Studies Program of IMS (2009-2010). XAFS measurements were performed with the approval of PF-PAC (Nos. 2006G337 and 2008G188).

Supporting information for this article is available on the WWW under http://dx.doi.org/10.1002/anie.201205167.

© 2012 Wiley-VCH Verlag GmbH & Co. KGaA, Weinheim

Table 1: Catalytic performance of CeO_2, ZrO_2, $Ce_2Zr_2O_x$, and supported Ni catalysts (2 wt% Ni) in CH_4 steam reforming.[a]

Catalyst	CH_4 conv. [%]	H_2O conv. [%]	Selec. C [%] (CO/CO_2)	Selec. H [%] (H_2)
CeO_2	0	0	–/–	–
ZrO_2	0	0	–/–	–
$Ce_2Zr_2O_8$	0	0	–/–	–
$Ce_2Zr_2O_7$	0	0	–/–	–
NiO/CeO_2[b]	0	0	–/–	–
Ni/CeO_2[c]	26.0	33.5	71.2/28.8	93.6
NiO/ZrO_2[b]	0	0	–/–	–
Ni/ZrO_2[c]	30.2	40.2	67.0/33.0	92.9
NiO/CeO_2-ZrO_2[b,d]	0	0	–/–	–
Ni/CeO_2-ZrO_2[c,d]	42.1	44.9	93.3/6.7	95.5
$NiO/Ce_2Zr_2O_8$[b]	0	0	–/–	–
$Ni/Ce_2Zr_2O_7$[c,e]	74.0	80.9	90.7/9.3	91.0
$Ni/Ce_2Zr_2O_7$[c]	81.8	91.5	88.1/11.9	94.0
$Ni/Ce_2Zr_2O_7$[c,f]	94.2	96.2	97.9/2.1	95.9

[a] Catalyst 0.1 g, total flow rate = 24.5 mL min^{-1}, $CH_4/H_2O/He = 2.8/2.8/94.4$ (molar ratio), 923 K. Analyzed at 1 h on time-on-stream. H_2O conv. was calculated as $(CO + 2\times CO_2)$/supplied $H_2O \times 100\%$. CO selectivity = $CO/(CO+CO_2)\times 100\%$. CO_2 selectivity = $CO_2/(CO+CO_2)\times 100\%$. H_2 selectivity = $(H_2)/(2\times$consumed CH_4 + consumed $H_2O)\times 100\%$. [b] Calcined at 773 K. [c] Reduced with H_2 at 773 K. [d] CeO_2 and ZrO_2 were physically mixed and then Ni was supported. [e] 873 K. [f] 973 K.

tages over other Ni catalysts, such as a Ni/co-precipitated CeO_2-ZrO_2 catalyst, whose CH_4 conversion decreased with reaction time (91→87%) and H_2 selectivity was as low as 74–78% in the presence of 0.8% O_2 in the reaction feed.

CeO_2-ZrO_2 materials have oxygen storage/release capacity (OSC) and are widely used as promoters of automobile three-way catalysts. The most efficient CeO_2-ZrO_2 material in terms of OSC is a solid solution, which has an atomically ordered arrangement of Ce and Zr assigned to the κ-$Ce_2Zr_2O_8$ fluorite phase.[9] The κ-$Ce_2Zr_2O_8$ phase transforms to the pyrochlore-$Ce_2Zr_2O_7$ phase by H_2 reduction, and the redox transformation is reversible (Supporting Information, Figure S1). In the $Ce_2Zr_2O_7$, Ce^{3+} ions are 8-fold coordinated and Zr^{4+} ions are 6-fold coordinated.[10] In the transformation from κ-$Ce_2Zr_2O_8$ to pyrochlore-$Ce_2Zr_2O_7$, the number of coordinated oxygen atoms at Zr sites changes without a change in Zr valence, whereas at Ce sites, the valence of Ce changes without a change in the number of coordinated oxygen atoms. These observations were made by analyzing the time-resolved XAFS.[11] Thus, Ni nanoparticles may be affected by the oxygen content of $Ce_2Zr_2O_x$ ($x = 7$–8), while the nature of $Ce_2Zr_2O_x$ may also change depending on the oxygen content.

The CH_4 steam reforming activity of $Ni/Ce_2Zr_2O_x$ ($x = 7$–8) was found to strongly depend on the oxygen content x of the $Ce_2Zr_2O_x$ solid solution, and a discontinuous change was found at $x = 7.5$. Figure 1 shows the variation in the CH_4 steam reforming performance with oxygen content x, where the samples with $x < 7.5$ were active under the steady-state conditions, whereas those with $x \geq 7.5$ were inactive. The structures and electronic states of the $Ni/Ce_2Zr_2O_x$ catalysts with different oxygen contents were characterized by XRD,

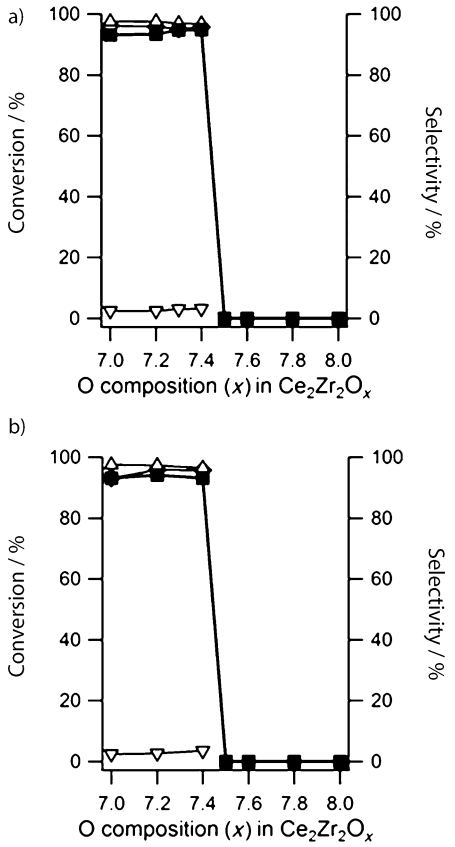

Figure 1. Catalytic performance of $Ni/Ce_2Zr_2O_x$ in CH_4 steam reforming at 973 K. a) Catalysts with different O content x prepared by the oxidation of Ni/pyrochlore-$Ce_2Zr_2O_7$ with a given amount of O_2 at 773 K, and b) catalysts with different O content x prepared by the reduction of NiO/κ-$Ce_2Zr_2O_8$ with a given amount of H_2 at 773 K. ■ (with bold line) CH_4 conversion [%], △ CO selectivity [%], ▽ CO_2 selectivity [%], ◇ H_2 selectivity [%].

Ni K-edge XANES and EXAFS, and Ce L_{III}-edge XANES and EXAFS.

TEM images for Ni (1 wt% and 2 wt%)/$Ce_2Zr_2O_7$ and Ni and Ce EDS profiles for Ni (2 wt%)/$Ce_2Zr_2O_7$ (Supporting Information, Figure S5) showed that Ni particles on the crystalline $Ce_2Zr_2O_7$ (roughly 700 nm size in average) with a low surface area of about 1 m^2 g^{-1} were as large as about 30 nm (average) even in the case of low Ni loadings of 1–2 wt%. It was hard to regulate Ni particle sizes to much smaller particles on the $Ce_2Zr_2O_x$ crystals.

Figure 2a shows the Ce L_{III}-edge XANES spectra of the $Ce_2Zr_2O_x$ phases in Ni/pyrochlore-$Ce_2Zr_2O_7$, $NiO_y/Ce_2Zr_2O_{7.4}$ prepared by oxidation of NiO/pyrochlore-$Ce_2Zr_2O_7$, $NiO_y/Ce_2Zr_2O_{7.4}$ prepared by reduction of NiO/κ-$Ce_2Zr_2O_8$ with a given amount of H_2 at 773 K, $NiO_y/Ce_2Zr_2O_{7.4}$ and $NiO_y/Ce_2Zr_2O_{7.6}$ prepared by oxidation of Ni/pyrochlore-$Ce_2Zr_2O_7$ with a given amount of O_2 at 773 K, and NiO/κ-$Ce_2Zr_2O_8$. The active $Ni/Ce_2Zr_2O_7$ catalyst showed no change in its XANES spectra before or after CH_4 steam reforming at 923 K. The Ce L_{III}-edge XANES data revealed that $Ce_2Zr_2O_{7.4}$ prepared by oxidation of $Ni/Ce_2Zr_2O_7$ was reduced to $Ce_2Zr_2O_7$ after CH_4 steam reforming. A similar change was observed for $NiO_y/Ce_2Zr_2O_{7.4}$ prepared by reduction of NiO/κ-$Ce_2Zr_2O_8$.

 © 2012 Wiley-VCH Verlag GmbH & Co. KGaA, Weinheim

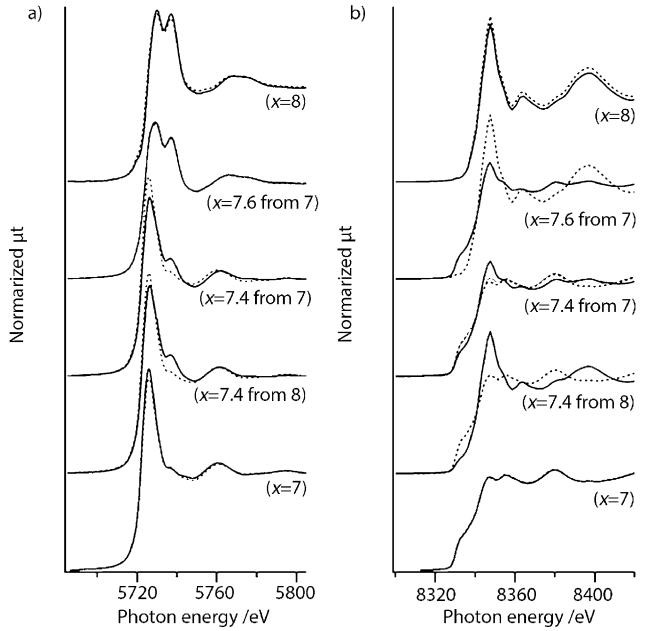

Figure 2. a) Ce L_{III}-edge and b) Ni K-edge XANES spectra of $NiO_y/Ce_2Zr_2O_x$ catalysts before and after CH_4 steam reforming. ($x=7$) Ni/pyrochlore-$Ce_2Zr_2O_7$, ($x=7.4$ from 8) $NiO_y/Ce_2Zr_2O_{7.4}$ prepared by H_2 reduction of NiO/κ-$Ce_2Zr_2O_8$, ($x=7.4$ from 7) $NiO_y/Ce_2Zr_2O_{7.4}$ prepared by O_2 oxidation of Ni/pyrochlore-$Ce_2Zr_2O_7$, ($x=7.6$ from 7) $NiO_y/Ce_2Zr_2O_{7.6}$ prepared by O_2 oxidation of Ni/pyrochlore-$Ce_2Zr_2O_7$, and ($x=8$) NiO/κ-$Ce_2Zr_2O_8$. Solid line: fresh catalyst; dotted line: catalyst after CH_4 steam reforming at 923 K; and gray solid line for ($x=7.4$ from 7) of (b): $NiO_y/Ce_2Zr_2O_{7.4}$ catalyst after treatment with CH_4 at 923 K in the absence of H_2O.

The phase transformation of $Ce_2Zr_2O_{7.4}$ after CH_4 steam reforming was also observed by XRD analysis (Figure 3). Fresh $NiO_y/Ce_2Zr_2O_{7.4}$ samples prepared by Ni/$Ce_2Zr_2O_7$ oxidation and by NiO/$Ce_2Zr_2O_8$ reduction showed almost the same XRD peaks at intermediate positions between

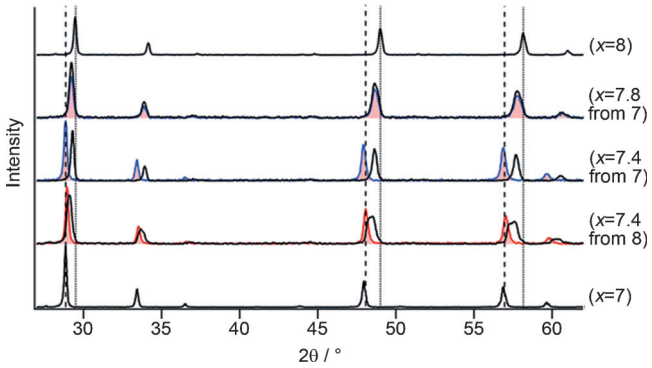

Figure 3. XRD patterns of $NiO_y/Ce_2Zr_2O_x$. ($x=7$) Ni/pyrochlore-$Ce_2Zr_2O_7$, ($x=7.4$ from 8) $NiO_y/Ce_2Zr_2O_{7.4}$ prepared by H_2 reduction of NiO/κ-$Ce_2Zr_2O_8$, ($x=7.4$ from 7) $NiO_y/Ce_2Zr_2O_{7.4}$ prepared by O_2 oxidation of Ni/pyrochlore-$Ce_2Zr_2O_7$ ($x=7.8$ from 7) $NiO_y/Ce_2Zr_2O_{7.8}$ prepared by O_2 oxidation of Ni/pyrochlore-$Ce_2Zr_2O_7$, and ($x=8$) NiO/κ-$Ce_2Zr_2O_8$. Black lines: fresh catalyst; red lines, red shading: catalyst after CH_4 steam reforming at 923 K; blue line: catalyst after the treatment with CH_4 at 923 K. Dashed and dotted lines: peak positions of pyrochlore-$Ce_2Zr_2O_7$ and κ-$Ce_2Zr_2O_8$, respectively.

pyrochlore-$Ce_2Zr_2O_7$ and κ-$Ce_2Zr_2O_8$. These XRD peaks shifted to the position corresponding to pyrochlore-$Ce_2Zr_2O_7$ after CH_4 steam reforming at 923 K. A similar transformation of $Ce_2Zr_2O_{7.4}$ to pyrochlore-$Ce_2Zr_2O_7$ also occurred with exposure to CH_4 without H_2O at 923 K.

In contrast, the Ce L_{III}-edge XANES spectrum of $NiO_y/Ce_2Zr_2O_{7.6}$ remained unchanged after CH_4 steam reforming (Figure 2a). The XRD of $NiO_y/Ce_2Zr_2O_{7.8}$ also showed no change after the reforming (Figure 3). There was also no change in the XANES spectrum of NiO/$Ce_2Zr_2O_8$ under the reforming conditions. Thus, the $Ce_2Zr_2O_x$ phase transformation proceeded depending on the oxygen content x of $Ce_2Zr_2O_x$, and the pyrochlore-$Ce_2Zr_2O_7$ phase was crucial for the high reforming activity. No XRD peak corresponding to crystalline Ni or NiO_y was observed in any sample.

The surface layers of Ni nanoparticles on $Ce_2Zr_2O_x$ should be oxidized to NiO in samples prepared by the O_2 oxidation of Ni/$Ce_2Zr_2O_7$, whereas these layers should be reduced to metallic Ni in samples prepared by the H_2 reduction of NiO/$Ce_2Zr_2O_8$. Thus, Ni nanoparticle surfaces in $NiO_y/Ce_2Zr_2O_x$ can have different Ni phases even in the same x. We characterized the Ni phase in $NiO_y/Ce_2Zr_2O_x$ by Ni K-edge XANES (Figure 2b). The XANES of Ni/$Ce_2Zr_2O_7$ was almost the same as that of Ni foil, which indicates that Ni nanoparticles on pyrochlore-$Ce_2Zr_2O_7$ are metallic. The Ni K-edge EXAFS analysis also revealed that the Ni nanoparticles were metallic Ni species, the Ni–Ni coordination number of which was 11.1 ± 1.3 at 0.249 ± 0.001 nm (Supporting Information, Table S1 and Figure S3).

As the white-line intensity at the Ni K-edge corresponds to the vacancy of Ni 3d levels, the Ni K-edge XANES spectra of the two $NiO_y/Ce_2Zr_2O_{7.4}$ samples indicate that Ni nanoparticles in $NiO_y/Ce_2Zr_2O_{7.4}$ prepared by the reduction of NiO/$Ce_2Zr_2O_8$ are more strongly oxidized than those in $NiO_y/Ce_2Zr_2O_{7.4}$ prepared by the oxidation of Ni/$Ce_2Zr_2O_7$. These results suggest that Ni nanoparticles in $NiO_y/Ce_2Zr_2O_{7.4}$ prepared by the oxidation of metallic Ni nanoparticles on pyrochlore-$Ce_2Zr_2O_7$ form a core–shell structure with a metallic Ni core and a NiO shell. On the other hand, Ni nanoparticles in $NiO_y/Ce_2Zr_2O_{7.4}$ prepared by the reduction of NiO nanoparticle on κ-$Ce_2Zr_2O_8$ form another core–shell structure with a NiO core and a metallic Ni shell. Although the core–shell phases in the two $NiO_y/Ce_2Zr_2O_{7.4}$ samples were different, both their Ni K-edge XANES spectra changed to that of metallic Ni nanoparticles in Ni/$Ce_2Zr_2O_7$ under the CH_4 steam reforming conditions (Figure 2b). Both $NiO_y/Ce_2Zr_2O_{7.4}$ catalysts also exhibited similar performance as shown in Figure 1. The activity of both $NiO_y/Ce_2Zr_2O_{7.4}$ catalysts was similar to that of Ni/$Ce_2Zr_2O_7$.

The Ni K-edge XANES spectrum of fresh $NiO_y(y=0.4)/Ce_2Zr_2O_{7.6}$ prepared by Ni/$Ce_2Zr_2O_7$ oxidation was not much different from that of fresh $NiO_y(y=0.3)/Ce_2Zr_2O_{7.4}$ prepared by Ni/$Ce_2Zr_2O_7$ oxidation (Figure 2b), where y was estimated from Ni K-edge white-line intensity. However, the $NiO_y/Ce_2Zr_2O_{7.6}$ catalyst showed no activity for the CH_4 steam reforming (Figure 1). The $NiO_y(y=0.3)/Ce_2Zr_2O_{7.4}$ sample was reduced to metallic Ni/$Ce_2Zr_2O_7$ under the CH_4 steam reforming conditions, whereas the $NiO_y(y=0.4)/Ce_2Zr_2O_{7.6}$ sample behaved similarly to NiO/$Ce_2Zr_2O_8$; that is, Ni

 © 2012 Wiley-VCH Verlag GmbH & Co. KGaA, Weinheim

nanoparticles were oxidized to NiO under the CH_4 steam reforming conditions (Figure 2b).

The high catalytic activity, robustness against deactivation, and newly found discontinuity may be related to the reactivity of lattice oxygen in $Ce_2Zr_2O_x$ ($7 \le x < 7.5$), to water activation to form protons and oxygen anions on the support surface, and to the strong interaction at the interface between Ni/NiO_y nanoparticles and the $Ce_2Zr_2O_x$ support ($7 \le x < 7.5$). On $NiO_y/Ce_2Zr_2O_x$($7.5 \le x \le 8$), an anti-phase boundary in the $Ce_2Zr_2O_x$ bulk suppresses oxygen diffusion and makes it difficult for water activation to occur.[12]

The discontinuity in catalytic performance at $x = 7.5$ may be related to the OSC of $Ce_2Zr_2O_x$[11] because it was not observed in the case of only NiO_y. The reduction of NiO_y strongly depended on the nature of the $Ce_2Zr_2O_x$ support. In the range of $7 \le x < 7.5$, Ni and $Ce_2Zr_2O_x$ were reduced to the metallic state and the pyrochlore-$Ce_2Zr_2O_7$ phase, respectively, under the reaction conditions; the reduction was due to CH_4. Indeed, the $NiO_y/Ce_2Zr_2O_{7.4}$ prepared from $Ni/Ce_2Zr_2O_7$ reacted with CH_4 in the absence of H_2O and was converted to $Ni/Ce_2Zr_2O_7$, as shown in Figure 2b and Figure 3. In the range of $7.5 \le x \le 8$, however, NiO_y was converted into NiO, and $Ce_2Zr_2O_x$ remained unchanged under the reaction conditions. The oxidation of Ni nanoparticles on $Ce_2Zr_2O_x$ ($7.5 \le x \le 8$) was due to H_2O.

In the range of $7 \le x < 7.5$, the reduction of the catalyst to $Ni/Ce_2Zr_2O_7$ by CH_4 was preferred over other reactions, whereas in $7.5 \le x \le 8$, the oxidation of the catalyst to $NiO/Ce_2Zr_2O_x$ by H_2O was preferred. No data for the Ellingham diagram of $Ce_2Zr_2O_x$ ($7 \le x \le 8$) are available,[13] but the dependence of the equilibrium pressure of oxygen (p_{O_2}) on the oxygen content x of $Ce_2Zr_2O_x$ shows different aspects at $x \ge 7.5$ and $x < 7.5$.[14] The oxygen storage and release processes rapidly occur at $x < 7.5$ compared with $x \ge 7.5$. A feature of kinetic catalyst bistability is seen in the present system, namely the tendency of the system to flip into two competing different redox states despite the presence of apparently unchanged thermodynamic gas phase conditions. In the range of $7 \le x < 7.5$, lattice oxygen atoms in $Ce_2Zr_2O_x$ readily migrate from the bulk to the surface, at which they react with CH_4 to form the resultant $Ce_2Zr_2O_7$ phase. This event occurs at the start of the reforming, followed by the catalytic CH_4 steam reforming that proceeds on the Ni/pyrochlore $Ce_2Zr_2O_7$ (produced in situ or initially prepared). NiO_y on $Ce_2Zr_2O_x$ may react directly with CH_4, but NiO_y on $Ce_2Zr_2O_{7.6}$ is not reduced. Thus, the direct reduction of NiO_y by CH_4 may be minor.

The transport of oxygen atoms at the interface between NiO_y nanoparticles and a $Ce_2Zr_2O_x$ support and/or the spillover of oxygen atoms at the boundary may be key issues in the chemical event of interest.[15] The NiO_y nanoparticles possess a disordered structure owing to strong interaction at the interface between the NiO_y and the $Ce_2Zr_2O_x$, which gives some strain to the nanoparticle structures (Supporting Information, Figure S5). Oxygen atoms move from NiO_y to $Ce_2Zr_2O_x$ at 923 K, thereby reducing NiO_y to metallic Ni, and $Ce_2Zr_2O_x$ to $Ce_2Zr_2O_7$, with CH_4. In the range of $7.5 \le x \le 8$, oxygen transport may be difficult owing to an increase in the energy barrier for oxygen diffusion in the bulk as a result of the anti-phase boundary.[13] CH_4 activation is difficult on the fluorite-type $Ce_2Zr_2O_x$ and the NiO produced on it.

CH_4 decomposition to C atoms may occur on the Ni surface, more preferably at the boundary of Ni nanoparticle and $Ce_2Zr_2O_x$ O-vacancy, followed by the reaction of C with H_2O or O anions produced by H_2O activation on the $Ce_2Zr_2O_x$ ($x < 7.5$) surface. The catalytic activity is considered to be a synergetic effect of the Ni and $Ce_2Zr_2O_x$ phases. The stable activity without significant coking may also be due to the OSC of the $Ce_2Zr_2O_x$ solid solution. Kinetic criticality phenomena are difficult to confirm and are usually highly resistant against monocausal explanations. Despite the macroscopic interpretation for the critical behavior, further study is needed for a micro-mechanistic unequivocal explanation of the observed discontinuity at $x = 7.5$. Nevertheless, the present finding of the discontinuous aspect and active phase in the new Ni/pyrochlore $Ce_2Zr_2O_7$ catalysis provides some implication to bifunctional catalyst design by synergetic interface, improving reactant activation and spillover of oxidizing/reducing species.

Experimental Section

Pyrochlore $Ce_2Zr_2O_7$ was prepared by co-precipitation using an aqueous NH_3 solution of $Ce(NO_3)_3{\cdot}6H_2O$ and $ZrO(NO_3)_2{\cdot}2H_2O$, followed by reduction with pure CO at 1673 K for 4 h.[9] The sample was calcined in air at 773 K for 3 h and impregnated with an aqueous solution of $Ni(NO_3)_2{\cdot}6H_2O$, followed by calcination at 773 K for 3 h to prepare $NiO/Ce_2Zr_2O_8$. $Ni/Ce_2Zr_2O_7$ was prepared by the reduction of $NiO/Ce_2Zr_2O_8$ with H_2 at 773 K for 3 h. CeO_2-ZrO_2 mixed oxides were prepared by co-precipitation of $ZrOCl_2$ and $(NH_4)_2Ce(NO_3)_2$ with $CO(NH_2)_2$ in a Teflon autoclave at 433 K for 4 h or by physical mixing of CeO_2 and ZrO_2, followed by calcination at 773 K, to which Ni was impregnated in a similar manner. Before use, the samples were reduced with H_2 at 773 K for 3 h. The details of the synthesis and characterization methods are described in the Supporting Information. XAFS spectra for the samples were measured at 293 K at KEK-PF (BL9A in a transmission mode (Ce L_{III}-edge) and BL12C in a fluorescence mode (Ni K-edge)).

CH_4 steam reforming reactions were conducted in a fixed-bed down-flow quartz-tube reactor of 6 mm inner diameter, typically using 0.1 g of catalyst at atmospheric pressure. The flow rates of H_2, CH_4, O_2, and He were regulated by mass flow controllers, and H_2O was supplied by bubbling of He. Reactants and products were analyzed two on-line GCs with columns packed with molecular sieves 5 A for H_2, O_2, CO, and CH_4 and Porapak-S for CO_2 and H_2O.

Received: July 2, 2012
Published online: August 21, 2012

Keywords: methane · nickel · solid solutions · steam reforming · XAFS

[1] J. Wei, E. Iglesia, *Angew. Chem.* **2004**, *116*, 3771; *Angew. Chem. Int. Ed.* **2004**, *43*, 3685.

[2] a) Y. H. Hu, E. Ruckerstein, *Catal. Rev.* **2002**, *44*, 423; b) J. R. Rostrup-Nielsen, J. Sehested, J. K. Norskov, *Adv. Catal.* **2002**, *47*, 65; c) A. T. Ashcroft, A. K. Cheetham, M. L. H. Green, P. D. F. Vernon, *Nature* **1991**, *352*, 225; d) S. Wang, G. Q. M. Lu, G. J. Millar, *Energy Fuels* **1996**, *10*, 896; e) M. C. J. Bradford, M. A. Vannice, *Catal. Rev. Sci. Eng.* **1999**, *41*, 1; f) A. P. E. York, T. C.

 © 2012 Wiley-VCH Verlag GmbH & Co. KGaA, Weinheim

Xiao, M. L. H. Green, J. B. Claridge, *Catal. Rev. Sci. Eng.* **2007**, *49*, 511; g) A. Yamaguchi, E. Iglesia, *J. Catal.* **2010**, *274*, 52; h) P. J. S. Prieto, A. P. Ferreira, P. S. Haddad, D. Zanchet, J. M. C. Bueno, *J. Catal.* **2010**, *276*, 351; i) M. H. Halabi, M. H. J. M. de Croon, J. van der Schaaf, P. D. Cobden, J. C. Schouten, *Appl. Catal. A* **2010**, *389*, 68; j) Y. Qu, A. M. Sutherland, J. Lien, G. D. Suarez, T. Guo, *J. Phys. Chem. Lett.* **2010**, *1*, 254; k) A. Martínez-Arias, M. Fernandez-Garcia, V. Ballesteros, L. N. Salamanca, J. C. Conesa, C. Otero, J. Soria, *Langmuir* **1999**, *15*, 4796; l) T. Choudhary, V. Choudhary, *Angew. Chem.* **2008**, *120*, 1852; *Angew. Chem. Int. Ed.* **2008**, *47*, 1828; m) R. Horn, K. A. Williams, N. J. Degenstein, L. D. Schmidt, *J. Catal.* **2006**, *242*, 92; n) D. K. Liguras, D. I. Kondarides, X. E. Verykios, *Appl. Catal. B* **2003**, *43*, 345.

[3] J. Wei, E. Iglesia, *J. Catal.* **2004**, *224*, 370.

[4] S. J. Blanksby, G. B. Ellison, *Acc. Chem. Res.* **2003**, *36*, 255.

[5] J. P. van Hook, *Catal. Rev. Sci. Eng.* **1980**, *21*, 1.

[6] a) C. E. Gigola, M. S. Moreno, I. Costilla, M. D. Sanchez, *Appl. Surf. Sci.* **2007**, *254*, 325; b) L. S. F. Feio, C. E. Hori, S. Damyanova, F. B. Noronha, W. H. Cassinelli, C. M. P. Marques, J. M. C. Bueno, *Appl. Catal. A* **2007**, *316*, 107; c) M. A. Ermakova, D. Y. Ermakov, G. G. Kuvshinov, L. M. Plyasova, *J. Catal.* **1999**, *187*, 77; d) S. Wang, G. Q. M. Lu, *Appl. Catal. B* **1998**, *19*, 267; e) J. B. Wang, Y. S. Wu, T. J. Huang, *Appl. Catal. A* **2004**, *272*, 289.

[7] a) J. S. Lee, S. T. Oyama, *Catal. Rev. Sci. Eng.* **1988**, *30*, 249; b) A. T. Ashcroft, A. K. Cheetham, J. S. Foord, M. L. H. Green, C. P. Grey, A. J. Murrell, P. D. F. Vernon, *Science* **1990**, *344*, 319; c) J. S. J. Hargreaves, G. J. Hutchings, R. W. Joyner, *Nature* **1990**, *348*, 428; d) M. Belgued, P. Pareja, A. Amariglio, H. Amariglio, *Nature* **1991**, *352*, 789; e) M. Lin, A. Sen, *Nature* **1994**, *368*, 613; f) R. A. Periana, D. J. Taube, S. Gamble, H. Tauble, T. Satoh, H. Fujii, *Science* **1998**, *280*, 560.

[8] J. Wei, E. Iglesia, *Phys. Chem. Chem. Phys.* **2004**, *6*, 3754.

[9] A. Suda, Y. Ukyo, H. Sobukawa, M. Sugiura, *J. Ceram. Soc. Jpn.* **2002**, *110*, 126.

[10] a) H. Kishimoto, T. Omata, S. Otsuka-Yao-Matsuo, K. Ueda, H. Hosono, H. Kawazoe, *J. Alloys Compd.* **2000**, *312*, 94; b) T. Sasaki, Y. Ukyo, K. Kuroda, S. Arai, S. Muto, H. Saka, *J. Ceram. Soc. Jpn.* **2004**, *112*, 440.

[11] T. Yamamoto, A. Suzuki, Y. Nagai, T. Tanabe, F. Dong, Y. Inada, M. Nomura, M. Tada, Y. Iwasawa, *Angew. Chem.* **2007**, *119*, 9413; *Angew. Chem. Int. Ed.* **2007**, *46*, 9253.

[12] S. Arai, S. Muto, T. Sasaki, K. Tatsumi, Y. Ukyo, K. Kuroda, H. Saka, *Solid State Commun.* **2005**, *135*, 664.

[13] T. B. Reed, *Free Energy of Formation of Binary Compounds: An Atlas of Charts for High-Temperature Chemical Calculations*, MIT Press, London, **1971**.

[14] S. Otsuka-Yao-Matsuo, N. Izu, T. Omata, K. Ikeda, *J. Electrochem. Soc.* **1998**, *145*, 1406.

[15] T. Schalow, M. Laurin, B. Brandt, S. Schauermann, S. Guimond, H. Kuhlenbeck, D. E. Starr, S. K. Shaikhutdinov, J. Libuda, H. J. Freund, *Angew. Chem.* **2005**, *117*, 7773; *Angew. Chem. Int. Ed.* **2005**, *44*, 7601.

 © 2012 Wiley-VCH Verlag GmbH & Co. KGaA, Weinheim